

Detachment scalings derived from 1D scrape-off-layer simulations

Thomas Body¹, Thomas Eich¹, Adam Kuang¹, Thomas Looby¹,
Mike Kryjak², Ben Dudson³, and Matt Reinke¹

¹Commonwealth Fusion Systems

²School of Physics, Engineering and Technology University of
York, Heslington, York YO10 5DD, UK

³Lawrence Livermore National Laboratory, 7000 East Avenue,
Livermore CA 94550, USA

April 2024

1 Abstract

Fusion power plants will require active detachment control to mitigate sputtering. Although detachment control has been demonstrated on current fusion experiments, achieving this on fusion power plants will be more challenging due to their reduced diagnostic set. Real-time scrape-off-layer (SOL) modeling will help to fill this "diagnostic gap". To determine the minimal set of physics required for accurate SOL modeling, we use the configurable Hermes-3 edge modeling framework to perform simple, fixed-fraction-impurity 1D Braginskii simulations. We show that these simulations reproduce distinctive attached and detached conditions, as well as the characteristic ion-flux rollover. We also perform scans of the input heat flux and impurity concentration, and show that the results predict similar trends to the lower-fidelity Lengyel model. This allows us to also indirectly compare to SOLPS simulations, and we find that the Lengyel model has similar "over-estimation" factors to Hermes-1D and SOLPS. This indirect comparison highlights a series of extensions to bring our Hermes-1D results closer to the higher-fidelity 2D modeling, with the goal of developing time-dependent detachment control suitable for next-generation fusion devices.

2 Introduction

Fusion power plants require stable divertor detachment to limit erosion of the divertor targets and keep heat fluxes within tolerable limits [Leo18]. This will require active feedback to control the detachment front location, including through

ramp-up, flat-top, ramp-down and during power transients such as H-L back-transitions. Feedback control of the detachment front location has been demonstrated on several existing devices, such as ASDEX Upgrade [Gru+95; Kal+12], JET [Mad+11], KSTAR [Eld+22], TCV [Rav+21], EAST [Xu+20] and W7-X [Jak+21], typically using either empirical control schemes or those based on simple models. However, on fusion power plants, the available diagnostic set will be significantly less than on existing devices [Rau+24], due to the high neutron flux, the need to increase the wall area available for tritium breeding, and the need to reduce complexity for commercial viability [Kua+18]. The reduced availability of diagnostics complicates detachment control on ARC [Kua+18], and to a degree also for SPARC [Rei+24]. Real-time scrape-off-layer modelling will help to fill the diagnostic gap for these devices.

Detachment modelling will be integrated into the plasma control system as well as real-time and near-real-time ‘flight’ simulators. One key use of detachment modelling will be to generate synthetic diagnostic signals for a range of possible plasma states. These will provide a basis for estimating the plasma state from multiple diagnostics, informing the necessary feedback response. Modelling could also be used to predict how the plasma will evolve in real-time, further constraining estimation of the plasma state and enabling preemptive control. Since there is a finite delay ($\sim 100ms$ in SPARC) between adjusting the gas injection rate and seeing a change in gas flow at the nozzle exit, preemptive control would have a significant advantage over proportional-only feedback if it could be made accurate enough for control. Accurate, real-time predictive modelling would let us control the future position of the detachment front, rather than its current location, and to also anticipate the plasma’s response to different gas injection waveforms. Within a model-predictive control [Sch+21] scheme, this could reduce the risk of reattachment or density-limit disruptions. This could be combined with full-system modelling and control — for instance, predicting the density increase due to a requested pellet injection and adjusting the gas-injection rate accordingly.

While there is a wealth of interpretive edge modelling available, the application of edge modelling for control is still under development. Rather than provide a complete review of the state-of-the-art, we provide here a few recent highlights demonstrating the application of detachment modelling for control. In Eldon et al., 2022 [Eld+22] the two-point-model was used to develop an improved detachment control scheme. This detachment controller was used on the KSTAR tokamak, and shown to improve the robustness to diagnostic noise and scenario changes compared to the previous control scheme. Another model being applied on KSTAR [Zha+23] is a machine-learned model developed in Zhu et al., 2022 [Zhu+22], where detachment control parameters have been linked to diagnostics using a large number of UEDGE simulations — although results using this model are not yet available. In Lore et al., 2023 [Lor+23] time-dependent SOLPS-ITER simulations were used to develop interrogable models which can be used within a model-predictive control framework, and work is ongoing to apply this modelling to SPARC [Par+24].

There is a significant increase in complexity and computational cost when going from simple models such as the two-point-model to complex 2D transport models such as SOLPS. To arrive at fast, intuitive models, there is significant benefit in determining the simplest possible model required to describe and control experimental conditions. To investigate this, we use the *configurable, open-source* Hermes edge modelling framework which lets us easily switch between different physical models, and even to vary the dimensionality of the simulation within a single framework. In this paper, we present our initial results from low-fidelity, fixed-fraction-impurity 1D Hermes modelling. This gives the first step in an investigation of detachment modelling across a range of fidelities, aiming at identifying a physics model for detachment control on SPARC.

3 Simulation setup

3.1 The model at a glance

We perform Hermes-1D simulations along a single flux-tube in the scrape-off-layer, starting at the outboard midplane and following a field line to the low-field-side divertor target. At the ‘upstream’ end of the flux-tube, particle and heat fluxes are added above the X-point, representing plasma transport from the confined region. The transport of energy and particles is then calculated according to the Braginskii equations projected into 1D [Bra65] (including ion thermal dynamics), giving a set of partial differential equations for the electron density, the electron and ion pressure, and the ion momentum¹. The equations solved are given as equations 2a) to 2c) in [Dud+24], with key features and differences outlined here. A no-flux boundary condition is applied upstream, and sheath boundary conditions and recycling ($R = 1$) are applied at the divertor target. A similar set of equations is used for the neutrals, with a pitch-angle-dependent increased parallel diffusion to approximate cross-field transport. As a rough approximation for pumping, we introduce a loss term for neutral particles $\frac{\partial n_d}{\partial t} = -n_d/\tau_{pump}$, where $\tau_{pump} \sim 100ms$ is estimated from SPARC’s effective pumping speed and volume.

In addition to energy loss at the divertor target, we use a ‘fixed-fraction’ impurity model to calculate the volumetric energy dissipation due to radiative cooling. At each point in the simulation, the local rate of cooling is calculated as $P_{cool} = c_z n_e^2 L_z(T_e)$ for a fixed c_z , with the radiative-cooling rate coefficients L_z computed for a fixed non-coronal parameter $n_e \tau = 10^{20}m^{-3} \cdot 0.5ms$, from Henderson et al., 2023 [Hen+23]². In this paper we use a neon impurity, but note that argon is also being considered as an edge radiator for SPARC.

¹The ion density is set equal to the electron density for singly-charged ions due to quasineutrality.

²For a discussion of the meaning of $n_e \tau$, see Mavrin 2017 [Mav17].

3.2 Detachment in Hermes-1D

The simulations are initialised with flat initial conditions and allowed to evolve in time until a quasi-steady-state is reached. This takes about $\sim 10ms$ of plasma time, requiring a few hours of computational time on a single CPU. As shown in figure 1, the simulations have distinctive 'attached' and 'detached' solutions³. In attached conditions the neutral density is negligible throughout the entire domain, and the plasma temperature rises smoothly away from the divertor targets. In detached conditions, there is a sharp interface between two distinct regions — one where the neutral density exceeds the plasma density and the plasma temperature drops to $\sim 1eV$, and another upstream of this where the solution looks similar to the attached case. Despite the significant difference in target conditions, the upstream conditions are remarkably similar. The detached case needed an upstream density just 27% higher than the attached case, and the corresponding drop in the upstream temperature was only 3% for the electrons and 10% for the ions⁴.

3.3 The transition from attached to detached conditions in Hermes-1D

To investigate the transition between attached and detached conditions in the simulation, we perform simulations with a time-varying power source and show the results in figure 2. The power is sinusoidally varied from 0.1 to $1.1GW/m^2$ with a period of $100ms$ for a constant input particle flux rate. The slow variation of q_{\parallel} was chosen such that the instantaneous solution is close to the steady-state solution.

We see that, as the power is decreased, the particle flux to the target initially increases due to the increasing target density. Then, at $0.4GW/m^2$, the target temperature levels out at $2eV$ and the target density begins to drop. This causes the target particle flux $\Gamma_{i,t}$ to roll over, which is a characteristic feature of detachment [KK17]. Interestingly, for a fixed input particle flux and pumping residence time, we also observe that the upstream density drops as the input power flux decreases. This may be a sign of *power starvation* [Ver+19], where the density drops as the power available for neutral ionisation is decreased. Alternatively, due to our model for pumping, the particle loss rate increases as the neutral density increases. For a fixed particle source rate, this will lead to

³Note that since the model is inherently simplified (i.e. lacking physics such as molecular recombination), one may debate whether these solutions accurately represent detachment. Nevertheless, we use the common terminology.

⁴Although the upstream densities are similar, the detached case required a $100\times$ higher input particle flux than the attached case. We can explain this qualitatively since we have set the particle loss rate proportional to the divertor neutral density, and so for a $\sim 10^5\times$ higher divertor neutral density, we need a correspondingly higher input particle flux. This estimate may suggest that we need an even larger change in the input particle flux, and indeed there is still a slow increase in the upstream density in the attached case of $\sim 20\%$ in $100ms$. Rather than continuing this simulation, a better pumping model such as the reservoir model discussed later will be pursued.

Hermes-1D: $q_{\parallel} = 1\text{GW}/\text{m}^{-2}$, $L_{\parallel} = 30\text{m}$, $c_{Ne} = 1\%$

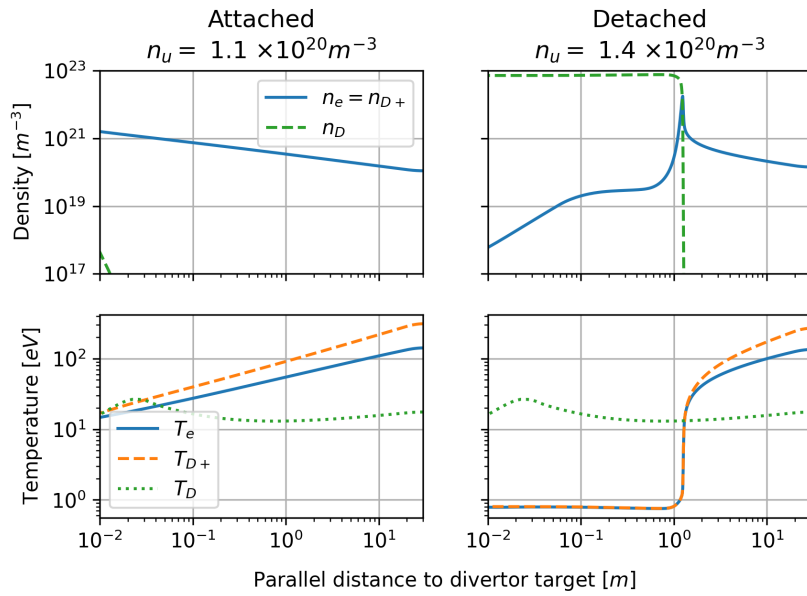


Figure 1: Two Hermes-1D simulations in steady state, showing an attached simulation (*left column*) and a detached simulation (*right column*). The *top row* gives the electron and neutral-deuterium densities, and the *bottom row* gives the electron, deuterium-ion and neutral-deuterium temperatures.

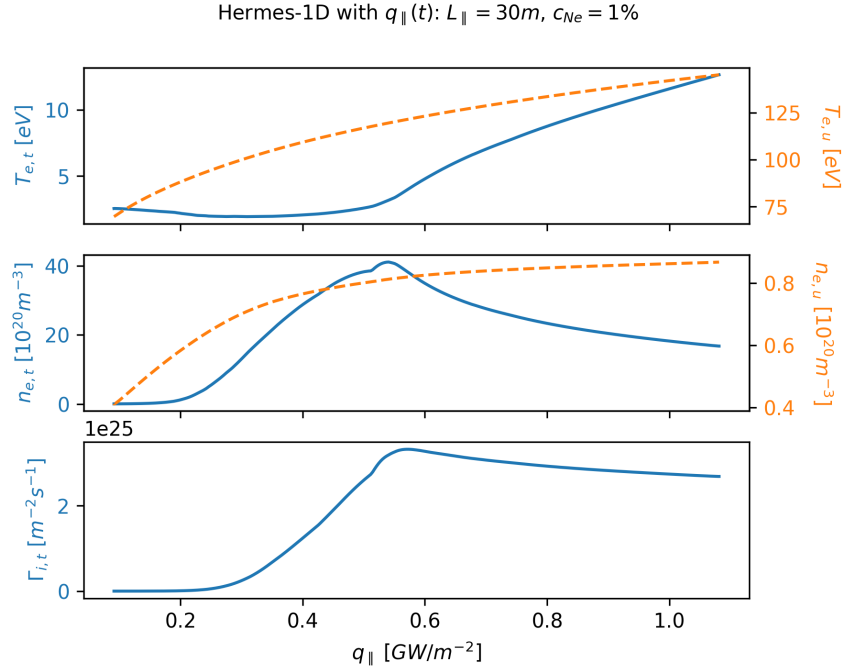


Figure 2: Target and upstream parameters from attached to detached conditions, giving the target (*blue-solid, left axis*) and upstream (*orange-dashed, right axis*) electron temperature (*top row*), density (*middle row*) and target particle flux (*bottom row*) as a function of the input parallel heat flux density q_{\parallel} .

a drop in the total number of particles — explaining at least in part the drop in upstream density.

Another notable feature of the results is the lack of a clear hysteresis: we find similar solutions at a given q_{\parallel} regardless of whether the heat flux is increasing or decreasing. For quasi-steady-state solutions, the separation of a 'cold-target' and 'hot-target' solution for a given q_{\parallel} is not observed in the simulation. We attempted to also perform a time-varying variation of the particle source, to enable a comparison to figure 1. However, we found that the system takes significantly longer to reach a steady-state for a changing input particle flux, and the variation in the particle flux needed to be significantly larger to clearly switch between attached and detached conditions.

3.4 Detachment scalings

Next, we want to study the relationship between the input heat flux density q_{\parallel} , the upstream density n_u (set by Γ_u), and the impurity concentration c_z for stably-detached conditions. Rather than adjusting these simulations by hand,

Hermes-1D with $L_{\parallel} = 30m$, $L_{det} = 1m$

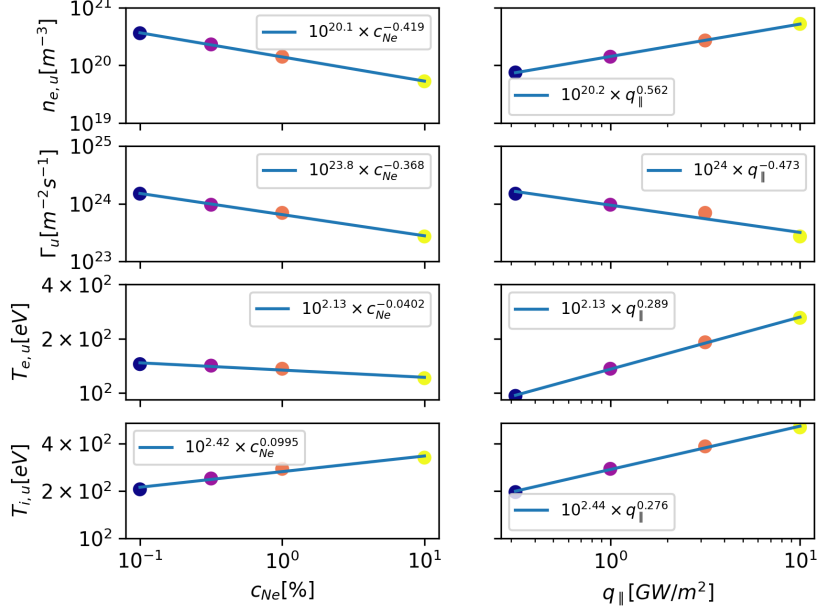


Figure 3: Upstream density (*top row*), input particle flux (*second row*), upstream electron temperature (*third row*) and upstream ion temperature (*bottom row*), for stable detachment as a function of the neon concentration (*left column*) and input power flux (*right column*). For the neon concentration scan, the power is held constant at $1GW/m^2$, and for the power flux scan the neon concentration is held constant at 1%. For each plot, simulation results are shown as coloured points and a power-law regression is shown as a solid line, with the regression given in the legend (in units given in the x- and y-labels).

we developed a PID controller [Bor+21] to control the position of the detachment front. This controller actively adjusts the input particle flux Γ_u to control the position where the neutral density crosses the electron density. As seen in figure 1, $n_d > n_e$ is sharply defined in the simulations and it is a robust indicator that volume recombination is occurring: as such, we define this as our detachment front location. The control parameters are determined using the Ziegler-Nichols method [ZN42; Bor+21], which were found to robustly determine a stable detachment point over a range of input parameters. The stability of the controller was further improved by resetting the integral term in the PID the first time the detachment front reaches its desired setpoint. This helps to counteract integral windup as the detachment front moves from the target to the setpoint. The complete implementation can be found at `hermes-3/src/detachment_controller.cxx`.

Using the detachment controller, we determined combinations of input parameters which result in stable detachment. In figure 3 we show the results for log-spaced values of q_{\parallel} from 0.1 to $10\text{GW}/\text{m}^2$, and for log-spaced values of c_{Ne} from 0.1% to 10%. For each simulation, the detachment controller aims to adjust the input particle flux until the detachment front is stabilised at a parallel distance of 1m to the divertor target. The controller is not always successful, and so in figure 3 we neglect simulations which have an error in the detachment front position of more than 0.1m .

We then perform regressions of the results. We find that the simulation results are well described by a power law, for both the impurity-concentration and heat flux scans. Combining the two, we find that

$$n_{e,u} \simeq 10^{20} \text{m}^{-3} \left(\frac{c_{Ne}}{1\%} \right)^{-0.419} \left(\frac{q_{\parallel}}{1\text{GW}/\text{m}^2} \right)^{0.562} \quad (1)$$

$$\Gamma_u \simeq 10^{24} \frac{\text{m}^{-2}}{\text{s}^{-1}} \left(\frac{c_{Ne}}{1\%} \right)^{-0.368} \left(\frac{q_{\parallel}}{1\text{GW}/\text{m}^2} \right)^{-0.473} \quad (2)$$

$$T_{e,u} \simeq 135\text{eV} \left(\frac{c_{Ne}}{1\%} \right)^{-0.0402} \left(\frac{q_{\parallel}}{1\text{GW}/\text{m}^2} \right)^{0.289} \quad (3)$$

$$T_{i,u} \simeq 270\text{eV} \left(\frac{c_{Ne}}{1\%} \right)^{0.0995} \left(\frac{q_{\parallel}}{1\text{GW}/\text{m}^2} \right)^{0.276} \quad (4)$$

3.5 Discussion and comparison to the Lengyel model

These regressions can be directly compared to the Lengyel model, which predicts $c_z \propto q_{\parallel}^{8/7} n_{e,u}^{-2}$ (see Appendix 1) and to Spitzer-Harm power balancing, which predicts $T_{e,u} \propto q_{\parallel}^{2/7}$. We see that the expected parametric dependencies agree remarkably well with the results of the regression — the analytical scalings $n_{e,u} \propto q_{\parallel}^{4/7=0.571}$ and $T_{e,u} \propto q_{\parallel}^{2/7=0.286}$ exactly match the scalings determined from Hermes, while the analytical $c_{Ne} \propto n_{e,u}^{-2}$ is slightly weaker than the $c_{Ne} \propto n_{e,u}^{-2.5}$ predicted by Hermes.

In addition to parameter scalings, the Lengyel model can also be used to predict the absolute concentration of the impurity concentration required to reach detachment. We implemented the Lengyel model in the open-source cf-SPOP CON framework and compare the results to the scalings derived from Hermes. In figure 4 we see that Hermes and the Lengyel model predict both similar parameter scalings (as expected from previous) and also similar absolute values. The highest degree of disagreement is found at high densities and low heating powers, where the Lengyel model predicts a $\sim 3\times$ higher impurity density than the Hermes scaling, and then a much lower impurity concentration at very high densities. We neglect the highest densities, since these fall outside the range for which we scanned with Hermes, and focus on the range with the highest overestimation factor. Under these conditions the convective heat flux becomes significant. This breaks the assumption in the Lengyel model that heat conduction is dominant, leading to disagreement between Hermes and the

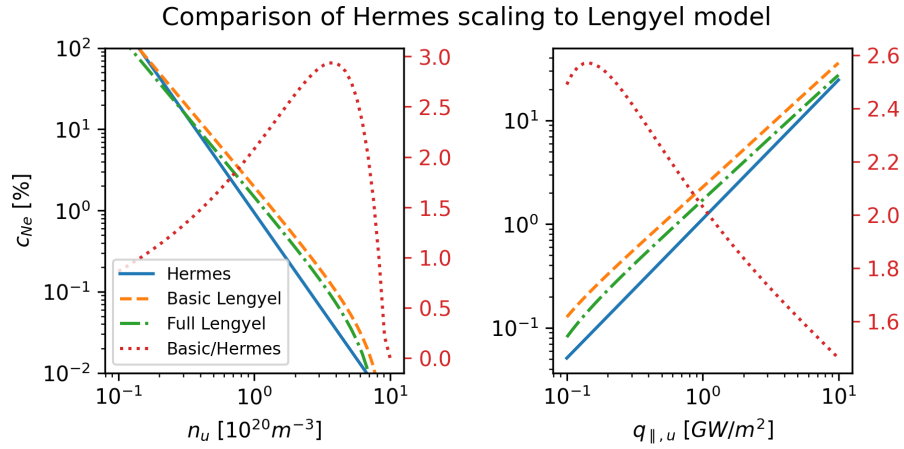


Figure 4: Neon concentration as a function of the upstream density (*left*) and input power flux (*right*). For the neon concentration scan, the power is held constant at $1GW/m^2$, and for the power flux scan the neon concentration is held constant at 1%. For each scan, the scaling derived from Hermes is shown as a *blue, solid* line. This is compared to results from the basic Lengyel model, shown as an *orange, dashed* line, and to the full Lengyel model, shown as a *green, dot-dashed* line. The ratio of the Hermes result to the basic Lengyel model is shown as a *red, dotted* line, and should be compared to the right-hand *red* axis.

Lengyel model. This result can also be compared to two recent comparisons of the Lengyel model to SOLPS 2D transport simulations. In Moulton et al., 2021 [Mou+21], the Lengyel model was found to estimate a $4.3\times$ higher impurity concentration than SOLPS-4.3 for neon-seeded ITER conditions. In Jarvinen et al., 2023 [Jär+23], the Lengyel model was found to estimate a factor of between 5 and $10\times$ higher impurity concentration than SOLPS-ITER for argon-seeded DEMO-ADC conditions. In both studies, the largest contribution to the deviation was the assumption of electron-conduction dominated heat transport in the Lengyel model. However, in addition to parallel convection, cross-field transport was also found to be important especially at temperatures around $\sim 10eV$, which may explain why the Hermes scaling lies between the Lengyel and SOLPS results. A useful extension would therefore be to treat the cross-field transport in Hermes 1D simulations, which has previously been shown to bring the results of 1D modelling (DIV1D) towards those of 2D transport [Der+22].

Other important extensions would be improved treatments of the impurity transport and neutrals. As noted in Moulton et al., 2021 [Mou+21], the assumption of a fixed $n_e\tau$ in the Lengyel model had the largest impact on the predicted inter-dependencies, since in SOLPS it was found that the impurity residence time τ increases with increasing upstream density and decreasing upstream ion temperatures. This effect could potentially be captured by adjusting $n_e\tau$ according to the upstream conditions or by modelling the transport of the impurity charge states. A further extension would be to improve the treatment of neutral particles to allow for transport outside of a single flux tube, such as via the neutral-reservoir model in Derks et al., 2024 [Der+24]. In DIV1D, combining this with a cross-field transport model leads to good agreement with SOLPS-ITER throughout a gas-puff scan on TCV [Der+24], and as such we plan to implement both these features in Hermes. Once a reasonable match to experiment is achieved, we will then investigate time-dependent detachment on existing tokamaks and use the model to develop detachment control schemes.

4 Conclusion

Reduced scrape-off-layer models are needed for detachment control on future fusion devices such as SPARC and ARC. In this work, we used the configurable Hermes framework to investigate detachment in a simple, fixed-fraction-impurity 1D Braginskii model. We show that the model is able to reproduce both attached and detached cases, as well as the transition between the two and the rollover of the ion saturation current. We then implemented a PID controller for the detachment position which holds the detachment front at a desired position. This enabled scans over the input power and impurity concentration, to determine the corresponding particle flux and upstream density which leads to stable detachment. The results of these scans are described by simple power-laws, which we then compare to the lower-fidelity Lengyel model. We find that the Lengyel model agrees reasonably closely with our scalings derived from Hermes, both in terms of magnitude and parametric inter-dependencies. The

largest disagreement — a factor of $\sim 3\times$ — is found at high densities and low input power, where we expect the convective contribution to the heat transport becomes significant. A similar result is found in SOLPS modelling, albeit with a larger factor, due to the additional strong contribution of cross-field transport at low temperatures. Future work will implement an effective model for cross-field transport, a neutral reservoir model and improved impurity transport modelling — focusing on developing an optimal physics model which enables fast, time-dependent and reasonably accurate scrape-off-layer modelling — in turn informing detachment control on next-step fusion devices.

5 Appendix 1: The Lengyel model

The Lengyel model was initially presented in a 1981 IPP report [Len81], and has since been presented in other references such as Reinke, 2017 [Rei17] and Moulton et al., 2021 [Mou+21].

If we assume the parallel heat-flux-density is carried only by electron conduction, we can write $q_{\parallel} = \kappa_{\parallel} T_e^{5/2} \frac{\partial T_e}{\partial s}$ for s a coordinate along a flux tube in the scrape-off-layer. If we add a fixed-fraction radiating impurity with a concentration of $c_z = n_z/n_e$, the change in q_{\parallel} due to radiative cooling will be $\frac{\partial q}{\partial s} = n_e n_z L_z(T_e) = n_e^2 c_z L_z(T_e)$ where $L_z(T_e)$ is the radiative cooling in Wm^3 (see Mavrin 2017 [Mav17] for a discussion of coronal and non-coronal radiative cooling curves). Therefore

$$q \frac{\partial q}{\partial s} = \kappa_{\parallel} T_e^{5/2} \frac{\partial T_e}{\partial s} n_e^2 c_z L_z(T_e)$$

Integrating along the fieldline from the target t to the upstream outboard-midplane u

$$\int_t^u q \partial q = \int_t^u \kappa_{\parallel} T_e^{5/2} n_e^2 c_z L_z(T_e) \partial T_e$$

If we assume that the static electron pressure is constant along most of the fieldline $n_e T_e = n_{e,u} T_{e,u}$

$$\frac{1}{2}(q_u^2 - q_t^2) = \kappa_{\parallel} n_{e,u}^2 T_{e,u}^2 c_z \int_t^u L_z(T_e) \sqrt{T_e} \partial T_e$$

As a shorthand, we denote $\int_t^u L_z(T_e) \sqrt{T_e} \partial T_e = L_{INT}$ and write the impurity concentration required as

$$c_z = \frac{q_u^2 - q_t^2}{2\kappa_{\parallel} n_{e,u}^2 T_{e,u}^2 L_{INT}}$$

The upstream density $n_{e,u}$ is a model input, while the upstream temperature $T_{e,u}$ can be determined in two ways. The first is via Spitzer-Harm power balancing $T_{e,u} = \left(T_{e,t} + \frac{7}{2} \frac{q_u L_{\parallel}}{\kappa_{\parallel}}\right)^{2/7}$ — which we refer to as the "basic Lengyel

model”. The second is by adjusting the upstream temperature so that it is consistent with $q_{\parallel} = \kappa_{\parallel} T_e^{5/2} \frac{\partial T_e}{\partial s}$. This is done by rearranging and integrating the heat flux equation, giving $L_{\parallel} = \kappa_{\parallel} \int_t^u T_e^{5/2} / q_{\parallel}(T_e) \partial T_e$ with $q_{\parallel}(T_e) = q_t^2 + 2\kappa_{\parallel} n_{e,u}^2 T_{e,u}^2 c_z \int_t^{T_e} L_z(T_e') \sqrt{T_e'} \partial T_e'$, and adjusting $T_{e,u}$ until L_{\parallel} matches the actual connection length. This in turn affects our calculation for c_z , so we iteratively solve for a consistent $(T_{e,u}, c_z)$ pair — which we refer to as the ”full Lengyel model”.

We can further simplify the basic Lengyel model by assuming $T_{e,t} \rightarrow 0, q_t \rightarrow 0$. Then, if we also assume an analytical form for L_{INT} , we can express c_z in a closed analytical form. Using $L_{INT} = m_L(Z, n_e \tau) T_{e,u}$ from Reinke 2017 [Rei17] and $T_u \propto q_u^{2/7}$ gives

$$c_z \propto q_u^2 (n_{e,u}^{-2} T_{e,u}^3)^{-1} \propto q_u^{8/7} n_{e,u}^{-2}$$

If we then assume an Eich scaling [Eic+13] such that $\lambda_q \sim B^{-1}$ then $q \sim \frac{PB}{R}$. Then, ignoring the extra factor of 1/7 on q_u , we can write $c_z \sim \left(\frac{PB}{R}\right) / n_{sep}^2$, which can be used as a metric for the challenge of reaching detachment.

6 Data availability

The software packages used for this paper are all publicly available. The results in this paper were generated using the following software versions (given as `software name`: git hash, link to software repository).

- `Hermes-3`: 8c45022 available from github.com/bendudson/hermes-3
- `cfsPOPCON`: 88e077f available from github.com/cfs-energy/cfspopcon
- `radas`: 92812df available from github.com/cfs-energy/radas

Input files and simulation results for this paper are available at 10.5281/zenodo.11484706.

7 Acknowledgements

This work was supported by Commonwealth Fusion Systems. Prepared in part by LLNL under Contract DE-AC52-07NA27344.

8 References

References

- [Bor+21] Rakesh P Borase et al. “A review of PID control, tuning methods and applications”. en. In: *Int. J. Dyn. Contr.* 9 (2 June 2021), pp. 818–827. DOI: 10.1007/s40435-020-00665-4. (Visited on 05/23/2024).

- [Bra65] Braginskii. “Transport Processes In A Plasma”. In: 1965.
- [Der+22] G L Derks et al. “Benchmark of a self-consistent dynamic 1D divertor model DIV1D using the 2D SOLPS-ITER code”. en. In: *Plasma Phys. Controlled Fusion* 64 (12 Nov. 11, 2022), p. 125013. DOI: 10.1088/1361-6587/ac9dbd. (Visited on 12/21/2022).
- [Der+24] G L Derks et al. “Multi-machine benchmark of the self-consistent 1D scrape-off layer model DIV1D from stagnation point to target with SOLPS-ITER”. en. In: *Plasma Phys. Control. Fusion* 66 (5 May 1, 2024), p. 055004. DOI: 10.1088/1361-6587/ad2e37. (Visited on 06/04/2024).
- [Dud+24] Ben Dudson et al. “Hermes-3: Multi-component plasma simulations with BOUT++”. In: *Computer Physics Communications* 296 (Mar. 1, 2024), p. 108991. DOI: 10.1016/j.cpc.2023.108991. (Visited on 04/22/2024).
- [Eic+13] T Eich et al. “Scaling of the tokamak near the scrape-off layer H-mode power width and implications for ITER”. en. In: *Nucl. Fusion* 53 (9 Aug. 29, 2013), p. 093031. DOI: 10.1088/0029-5515/53/9/093031.
- [Eld+22] D Eldon et al. “Enhancement of detachment control with simplified real-time modelling on the KSTAR tokamak”. In: *Plasma Phys. Control. Fusion* 64 (7 July 1, 2022), p. 075002. DOI: 10.1088/1361-6587/ac6ff9.
- [Gru+95] O Gruber et al. “Observation of continuous divertor detachment in H-mode discharges in ASDEX upgrade”. en. In: *Phys. Rev. Lett.* 74 (21 May 22, 1995), pp. 4217–4220. DOI: 10.1103/PhysRevLett.74.4217. (Visited on 05/03/2024).
- [Hen+23] Stuart Scott Henderson et al. “Divertor detachment and reattachment with mixed impurity seeding on ASDEX Upgrade”. en. In: *Nucl. Fusion* (June 29, 2023). DOI: 10.1088/1741-4326/ace2d6. (Visited on 07/04/2023).
- [Jak+21] M Jakubowski et al. “Overview of the results from divertor experiments with attached and detached plasmas at Wendelstein 7-X and their implications for steady-state operation”. en. In: *Nucl. Fusion* 61 (10 Aug. 30, 2021), p. 106003. DOI: 10.1088/1741-4326/ac1b68.
- [Jär+23] A E Järvinen et al. “Parametric scaling of power exhaust in EU-DEMO alternative divertor simulations”. In: *Nucl. Eng. Des./Fusion* 34 (Mar. 1, 2023), p. 101378. DOI: 10.1016/j.nme.2023.101378.
- [Kal+12] A Kallenbach et al. “Optimized tokamak power exhaust with double radiative feedback in ASDEX Upgrade”. en. In: *Nucl. Fusion* 52 (12 Nov. 14, 2012), p. 122003. DOI: 10.1088/0029-5515/52/12/122003.

- [KK17] S I Krasheninnikov and A S Kukushkin. “Physics of ultimate detachment of a tokamak divertor plasma”. In: *J. Plasma Phys.* 83 (5 Oct. 2017). DOI: 10.1017/S0022377817000654. (Visited on 06/12/2022).
- [Kua+18] A Q Kuang et al. “Conceptual design study for heat exhaust management in the ARC fusion pilot plant”. In: *Fusion Eng. Des.* 137 (Dec. 1, 2018), pp. 221–242. DOI: 10.1016/j.fusengdes.2018.09.007.
- [Len81] L L Lengyel. *Analysis of Radiating Plasma Boundary Layers*. Research rep. Max Planck Institute for Plasma Physics, 1981.
- [Leo18] A W Leonard. “Plasma detachment in divertor tokamaks”. en. In: *Plasma Phys. Controlled Fusion* 60 (4 Feb. 7, 2018), p. 044001. DOI: 10.1088/1361-6587/aaa7a9. (Visited on 06/12/2022).
- [Lor+23] J D Lore et al. “Time-dependent SOLPS-ITER simulations of the tokamak plasma boundary for model predictive control using SINDy”. In: *Nucl. Med.* (2023).
- [Mad+11] G P Maddison et al. “Demonstration of real-time control of impurity seeding plus outboard strike-point sweeping in JET ELMy H-mode plasmas”. en. In: *Nucl. Fusion* 51 (8 Aug. 8, 2011), p. 082001. DOI: 10.1088/0029-5515/51/8/082001.
- [Mav17] A A Mavrin. “Radiative Cooling Rates for Low-Z Impurities in Non-coronal Equilibrium State”. In: *J. Fusion Energy* 36 (4 Oct. 1, 2017), pp. 161–172. DOI: 10.1007/s10894-017-0136-z.
- [Mou+21] D Moulton et al. “Comparison between SOLPS-4.3 and the Lengyel Model for ITER baseline neon-seeded plasmas”. en. In: *Nucl. Fusion* 61 (4 Mar. 17, 2021), p. 046029. DOI: 10.1088/1741-4326/abe4b2. (Visited on 02/14/2023).
- [Par+24] Jae-Sun Park et al. “Full time-dependent SOLPS-ITER simulation of the SPARC tokamak: Actuator design for particle and divertor condition control”. en. In: *Nucl. Fusion* (May 23, 2024). DOI: 10.1088/1741-4326/ad4f9d. (Visited on 05/28/2024).
- [Rau+24] J Raukema et al. “Demonstration of a sparse sensor placement technique to the limited diagnostic set in a fusion power plant”. en. In: *Fusion Eng. Des.* 201 (114271 Apr. 2024), p. 114271. DOI: 10.1016/j.fusengdes.2024.114271.
- [Rav+21] T Ravensbergen et al. “Real-time feedback control of the impurity emission front in tokamak divertor plasmas”. en. In: *Nat. Commun.* 12 (1 Feb. 17, 2021), p. 1105. DOI: 10.1038/s41467-021-21268-3.
- [Rei+24] Matt Reinke et al. “Overview of the Early Campaign Diagnostics for the SPARC Tokamak”. In: *Rev. Sci. Instrum.* (2024).
- [Rei17] M L Reinke. “Heat flux mitigation by impurity seeding in high-field tokamaks”. en. In: *Nucl. Fusion* 57 (3 Jan. 13, 2017), p. 034004. DOI: 10.1088/1741-4326/aa5145. (Visited on 06/12/2022).

- [Sch+21] Max Schwenzer et al. “Review on model predictive control: an engineering perspective”. en. In: *Int. J. Adv. Manuf. Technol.* 117 (5-6 Nov. 11, 2021), pp. 1327–1349. DOI: 10.1007/s00170-021-07682-3. (Visited on 05/23/2024).
- [Ver+19] K Verhaegh et al. “An improved understanding of the roles of atomic processes and power balance in divertor target ion current loss during detachment”. en. In: *Nucl. Fusion* 59 (12 Oct. 17, 2019), p. 126038. DOI: 10.1088/1741-4326/ab4251.
- [Xu+20] G S Xu et al. “Divertor impurity seeding with a new feedback control scheme for maintaining good core confinement in grassy-ELM H-mode regime with tungsten monoblock divertor in EAST”. en. In: *Nucl. Fusion* 60 (8 Aug. 1, 2020), p. 086001. DOI: 10.1088/1741-4326/ab91fa. (Visited on 04/22/2024).
- [Zha+23] Menglong Zhao et al. “Building database of 2D UEDGE simulations for KSTAR detachment control”. In: *APS Division of Plasma Physics Meeting Abstracts*. Vol. 2023. APS Meeting Abstracts. Jan. 2023, UP11.107.
- [Zhu+22] Ben Zhu et al. “Data-driven model for divertor plasma detachment prediction”. In: *J. Plasma Phys.* 88 (5 Oct. 2022), p. 895880504. DOI: 10.1017/S002237782200085X. (Visited on 01/17/2023).
- [ZN42] J G Ziegler and N B Nichols. “Optimum settings for automatic controllers”. en. In: *Journal of Fluids Engineering* 64 (8 Nov. 1, 1942), pp. 759–765. DOI: 10.1115/1.4019264.